Exploring Local Graphs via Random Encoding for Texture Representation Learning

Ricardo T. Fares[a], Luan B. Guerra[b] and Lucas C. Ribas[c]
São Paulo State University (UNESP), Institute of Biosciences, Humanities and Exact Sciences, São José do Rio Preto, Brazil
{rt.fares, luan.bonizi, lucas.ribas}@unesp.br

Keywords: Texture Representation, Randomized Neural Networks, Graph-Based Modeling.

Abstract: Despite many graph-based approaches being proposed to model textural patterns, they not only rely on a large number of parameters, culminating in a large search space, but also model a single, large graph for the entire image, which often overlooks fine-grained details. This paper proposes a new texture representation that utilizes a parameter-free micro-graph modeling, thereby addressing the aforementioned limitations. Specifically, for each image, we build multiple micro-graphs to model the textural patterns, and use a Randomized Neural Network (RNN) to randomly encode their topological information. Following this, the network's learned weights are summarized through distinct statistical measures, such as mean and standard deviation, generating summarized feature vectors, which are combined to form our final texture representation. The effectiveness and robustness of our proposed approach for texture recognition was evaluated on four datasets: Outex, USPtex, Brodatz, and MBT, outperforming many literature methods. To assess the practical application of our method, we applied it to the challenging task of Brazilian plant species recognition, which requires microtexture characterization. The results demonstrate that our new approach is highly discriminative, indicating an important contribution to the texture analysis field.

1 INTRODUCTION

Texture is an essential attribute present in numerous natural objects and scenes. Despite the absence of a formally established definition of texture, it can be understood as the spatial layout of intensities within a local neighborhood of a pixel. In living beings, the visual cortex is responsible for processing and encoding textural information into complex representations, enabling the recognition of various surfaces and materials (Jagadeesh and Gardner, 2022). To bring similar recognition capabilities to computers, researchers have developed texture descriptors that numerically express these features in one-dimensional vectors, enabling its application in numerous tasks, such as tissue classification (Kruper et al., 2024), environment monitoring (Borzooei et al., 2024) and remote sensing (Xu et al., 2024).

Initially, automated texture encoding approaches relied on classical or hand-engineered methods, in which the textural encoding processes were manually designed by specialists. Examples of such approaches include: the Gray-Level Co-occurrence Matrix (GLCM) (Haralick, 1979), which extracts k-th order statistical information to describe the distribution of local patterns of the pixel neighborhoods, and Local Binary Patterns (LBP) (Ojala et al., 2002b), which encodes pixel neighborhoods into unique values that are then aggregated into a histogram. However, due to the increasing complexity of images generated by diverse real-world applications, these approaches often struggle to handle this complexity and fail to achieve satisfactory results.

To address this, various learning-based approaches have been developed that rely on large artificial neural networks, such as Convolutional Neural Networks (CNNs) and Vision Transformers (ViTs), which automatically learn to extract useful visual features by minimizing a loss function. Examples of such architectures are: VGG19 (Simonyan and Zisserman, 2014), InceptionV3 (Szegedy et al., 2016), ResNet50 (He et al., 2016), and InceptionResNetV2 (Szegedy et al., 2017). Although these models have achieved superior results across many tasks, they are often constrained by limited training data, a challenge commonly encountered in certain applications, such

[a] https://orcid.org/0000-0001-8296-8872
[b] https://orcid.org/0009-0004-3278-9306
[c] https://orcid.org/0000-0003-2490-180X

Fares, R. T., Guerra, L. B. and Ribas, L. C.
Exploring Local Graphs via Random Encoding for Texture Representation Learning.
DOI: 10.5220/0013315500003912

In *Proceedings of the 20th International Joint Conference on Computer Vision, Imaging and Computer Graphics Theory and Applications (VISIGRAPP 2025) - Volume 3: VISAPP*, pages 200-209
ISBN: 978-989-758-728-3; ISSN: 2184-4321

as medicine, which can lead to optimization issues.

In this sense, to harness the advantages of hand-engineered approaches, known for their invariance to the need for large datasets, alongside the automatic feature extraction of learning-based approaches, recent texture representation techniques have employed randomized neural networks (RNNs) (Sá Junior and Backes, 2016; Ribas et al., 2024a; Fares and Ribas, 2024) for pattern recognition tasks. These networks are both simple and fast-learning, as their training phase is conducted via a closed-form solution, eliminating the need for backpropagation. In these investigations, a randomized neural network is trained for each image, with the learned weights used to construct the texture representation. However, the effectiveness of this texture descriptor largely depends on the construction of the input feature matrix (local patches), which provides the information to be randomly encoded.

In particular, several RNN-based approaches, such as in (Ribas et al., 2020; Ribas et al., 2024a; Ribas et al., 2024b) use *graphs*, a well-known mathematical tool, to model relationships among textural patterns in the image. However, the graph modeling in these approaches requires between 1 and 4 hyper-parameters to be calibrated, resulting in a large search space of parameter combinations. Additionally, these approaches model the entire image as a single large graph, which may overlook finer texture details and introduce scalability issues due to the graph size relative to image resolution.

In this paper, we introduce a novel texture representation approach that (1) employs hyperparameter-free graph modeling by utilizing multiple micro-graphs to capture local textural information in the image; and (2) uses randomized neural networks to randomly encode these micro-graphs in the network's learned weights. Specifically, to build the representation, we center a 3×3 local patch on each pixel of the image, construct a micro-graph to model this patch, and extract topological measures. From this, the pixel intensities of the patches form the input feature matrix, and the topological measures of the modeled graph the output one. These matrices are then used to feed a randomized neural network (RNN), where the network's learned weights are summarized using statistical measures. Each statistical measure generates a distinct statistical vector, which is then combined to compose our final texture representation. In summary, the main contributions of our work are: (i) A parameter-free graph modeling approach. (ii) A compact and low-cost representation via RNNs. (iii) Invariance to the dataset size. (iv) Promising results in the challenging task of Brazilian plant species recognition.

Finally, the paper is organized as follows. In Section 2, we describe the proposed methodology. In Section 3, we present the experimental setup, results, discussion, and comparisons. Lastly, in Section 4 we conclude the paper.

2 PROPOSED METHOD

2.1 Randomized Neural Networks

Randomized neural network is a simple neural network model composed by a single fully-connected hidden layer whose weights are randomly generated by some probability distribution (Huang et al., 2006; Pao and Takefuji, 1992; Pao et al., 1994; Schmidt et al., 1992). The objective is to randomly project the input into a higher dimensional space, thereby enhancing the probability of the data becoming more linearly separable, as stated in Cover's theorem (Cover, 1965). Following this, the weights of the output layer are learned through a closed-form solution, i.e. gradient-free, to minimize a least-squares error optimization problem.

Mathematically, let $\mathbf{X} = [\vec{x}_1, \vec{x}_2, \ldots, \vec{x}_N] \in \mathbb{R}^{p \times N}$, where $\vec{x}_i \in \mathbb{R}^p$ be the input feature matrix composed of N input feature vectors, and let $\mathbf{Y} = [\vec{y}_1, \vec{y}_2, \ldots, \vec{y}_N] \in \mathbb{R}^{r \times N}$, where $\vec{y}_i \in \mathbb{R}^r$ be the output feature matrix consisting of N output feature vectors. Further, let $\mathbf{W} \in \mathbb{R}^{Q \times (p+1)}$ be the randomly generated weight matrix, with Q being the number of hidden neurons, and with the first column being the bias' weights. Lastly, let $\mathbf{1}_N$ be a row matrix with N columns with all entries set as 1, and define $\mathbf{X}' = [-\mathbf{1}_N^T \;\; \mathbf{X}^T]^T$ as the input feature matrix with the bias appended.

From this, we can compute the forward step by $\mathbf{U} = \phi(\mathbf{W}\mathbf{X})$, where ϕ is the sigmoid function, and $\mathbf{U} = [\vec{u}_1, \vec{u}_2, \ldots, \vec{u}_N] \in \mathbb{R}^{Q \times N}$, where $\vec{u} \in \mathbb{R}^Q$ is the matrix consisting of the N randomly projected input feature vectors in the Q-dimensional space. Further, we define $\mathbf{Z} = [-\mathbf{1}_N^T \;\; \mathbf{U}^T]^T$ as the projected feature matrix with the bias added.

From this, we can calculate the output layer weights by the following closed-solution formula:

$$\mathbf{M} = \mathbf{Y}\mathbf{Z}^T(\mathbf{Z}\mathbf{Z}^T)^{-1}, \tag{1}$$

where $\mathbf{Z}^T(\mathbf{Z}\mathbf{Z}^T)^{-1}$ is the Moore-Penrose pseudo-inverse (Moore, 1920; Penrose, 1955). Nevertheless, there may be cases where $\mathbf{Z}\mathbf{Z}^T$ is ill-conditioned, producing unstable inverses. To tackle this issue, Tikhonov regularization (Tikhonov, 1963; Calvetti et al., 2000) is applied, by adjusting the formula to:

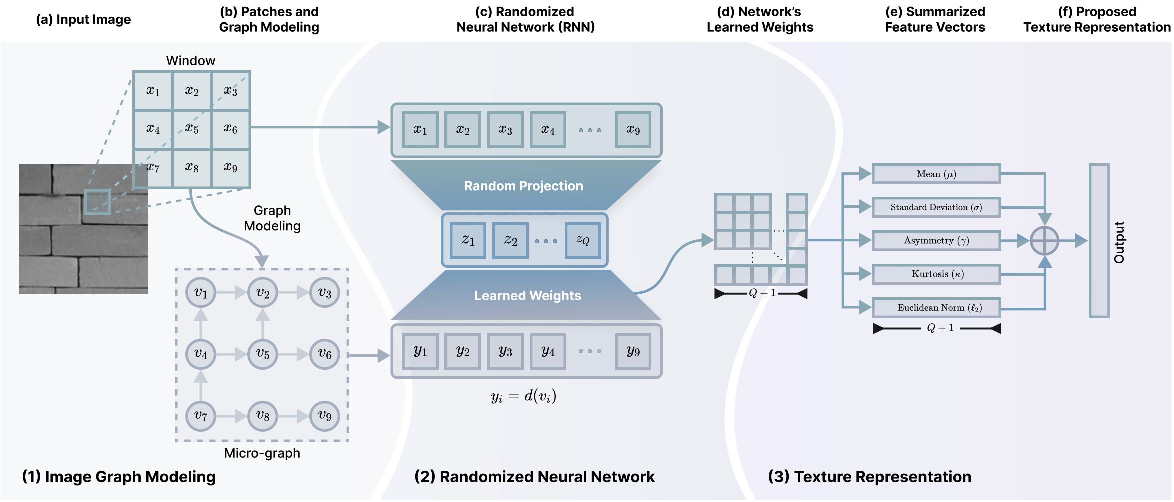
(a) Input Image
(b) Patches and Graph Modeling
(c) Randomized Neural Network (RNN)
(d) Network's Learned Weights
(e) Summarized Feature Vectors
(f) Proposed Texture Representation
Window
x_1 x_2 x_3
x_4 x_5 x_6
x_7 x_8 x_9
Graph Modeling
v_1 v_2 v_3
v_4 v_5 v_6
v_7 v_8 v_9
Micro-graph
x_1 x_2 x_3 x_4 ... x_9
Random Projection
z_1 z_2 ... z_Q
Learned Weights
y_1 y_2 y_3 y_4 ... y_9
$y_i = d(v_i)$
$Q+1$
Mean (μ)
Standard Deviation (σ)
Asymmetry (γ)
Kurtosis (κ)
Euclidean Norm (ℓ_2)
$Q+1$
Output
(1) Image Graph Modeling
(2) Randomized Neural Network
(3) Texture Representation

Figure 1: Illustration of the process to obtain the texture representation from the (a) input image to (f) the proposed texture representation. The steps include (b) micro-graph modeling of the local patches, which are then applied to a (c) RNN to produce the (d) network's learned weights. These weights are (e) summarized and subsequently combined to form the (f) proposed texture representation.

$\mathbf{M} = \mathbf{Y}\mathbf{Z}^T(\mathbf{Z}\mathbf{Z}^T + \lambda\mathbf{I})^{-1}$, where $\lambda > 0$ is the regularization parameter, and $\mathbf{I} \in \mathbb{R}^{(Q+1)\times(Q+1)}$ is the identity matrix. Finally, we set $\lambda = 10^3$ as suggested in other investigations (Fares et al., 2024).

2.2 Learning Texture Representation

The key idea underlying our approach is that, unlike other graph-based methods that construct a single large graph to model the entire image texture, we instead create multiple micro-graphs centered on each pixel of the image, enabling us to capture finer texture details. We then extract topological measures from these micro-graphs and use them in a randomized neural network. Finally, the network's learned weights are summarized to construct the texture representation.

To construct the representation of an image $I \in \mathbb{R}^{H\times W}$, we start by creating the input feature matrix $\mathbf{X}$ and the output feature matrix $\mathbf{Y}$. For each pixel in I, we center a 3×3 window to capture their local spatial relationships, flatten and concatenate them to form the matrix $\mathbf{X} \in \mathbb{R}^{9\times HW}$. Furthermore, each window is modeled as a micro-graph composed by 9 vertices (one per pixel) with a directed edge e_{ij} going from vertex v_i to v_j when $P(v_i) > P(v_j)$, where $P(v)$ denotes the intensity level of the pixel corresponding to the vertex v (note that micro-graph in Figure 1(b) illustrates only some edges, to not clutter the image). This micro-graph is then converted into a vector containing the out-degrees of each vertex, where the out-degree $d(v)$ is the number of outgoing edges from v. This process produces a vector per local window, and by concatenating these vectors across all windows, we form the matrix $\mathbf{Y} \in \mathbb{R}^{9\times HW}$. This process is depicted in Figure 1(a) and 1(b).

With $\mathbf{X}$ and $\mathbf{Y}$ constructed, we applied it to a randomized neural network and obtained the network's learned weights, $\mathbf{M}$, using the regularized form of Equation 1. These learned weights capture essential information about the textural content encoded by the pixel intensities and topological measures (e.g., out-degrees), as the network is trained to predict one using the other. Thus, from this matrix, we defined our following summarized feature vector:

$$\vec{\Theta}_f(Q) = [f(\vec{m}_1), f(\vec{m}_2), \ldots, f(\vec{m}_{Q+1})], \quad (2)$$

where f is a statistical measure function (μ for average, σ for standard deviation, γ for skewness, κ for kurtosis, and ℓ for ℓ_2 norm squared), $\vec{m}_k$ denotes the k-th column of the matrix $\mathbf{M}$, and $f(\vec{m}_k)$ indicates the measure function applied over the values at the k-th column.

From this, we create the partial feature vector by incorporating different statistical measure functions. In particular, we applied four statistical measures: average, standard deviation, skewness and kurtosis (see Table 1), and one ℓ_2 norm function. This approach positively contributes to the representation, as different statistical perspectives are taken into account, as investigated in (Fares et al., 2024). Thus, we define it as:

$$\vec{\Omega}(Q) = [\vec{\Theta}_\mu(Q), \vec{\Theta}_\sigma(Q), \vec{\Theta}_\gamma(Q), \vec{\Theta}_\kappa(Q), \vec{\Theta}_\ell(Q)]. \quad (3)$$

The representation $\vec{\Omega}(Q)$ is uniquely determined by Q, the dimension of the projection space.

Since different projection space dimensions randomly project the features in distinct ways, unique information can be captured during the prediction phase. Hence, we define our proposed texture representation as:

$$\vec{\Phi}(\mathbf{Q}) = [\vec{\Omega}(Q_1), \vec{\Omega}(Q_2), \ldots, \vec{\Omega}(Q_L)], \quad (4)$$

where $\mathbf{Q} = (Q_1, Q_2, \ldots, Q_L)$.

To conclude, feature extraction methods must ensure reproducibility by generating the same feature vector for the same input image in all executions. For this purpose, this investigation employed the same random weight matrix for projecting each input feature matrix across all images and runs. Specifically, as extensively employed in previously RNN-based investigations (Sá Junior and Backes, 2016; Ribas et al., 2020; Ribas et al., 2024b; Fares et al., 2024), the random matrix was generated using a Linear Congruent Generator (LCG), defined by the recurrent formula $V(n+1) = (aV(n)+b) \mod c$, where V is the vector of length $L = Q \times (p+1)$, with parameters $V(0) = L+1, a = L+2, b = L+3$, and $c = L^2$. Lastly, the vector V is standardized, and W is obtained by reshaping V into $(Q, p+1)$ dimensions.

Table 1: Statistical measures formulas utilized to summarize the network's learned weights.

Average	Standard Deviation
$\mu(\vec{v}) = \frac{1}{N}\sum_{k=1}^{N} v_k$	$\sigma(\vec{v}) = \sqrt{\frac{1}{N-1}\sum_{k=1}^{N}(v_k - \mu(\vec{v}))^2}$
Skewness	
$\gamma(\vec{v}) = \frac{\frac{1}{N}\sum_{k=1}^{N}(v_k-\mu(\vec{v}))^3}{\left(\sqrt{\frac{1}{N-1}\sum_{k=1}^{N}(v_k-\mu(\vec{v}))^2}\right)^3}$	
Kurtosis	
$\kappa(\vec{v}) = \frac{\frac{1}{N}\sum_{k=1}^{N}(v_k-\mu(\vec{v}))^4}{\left(\sqrt{\frac{1}{N-1}\sum_{k=1}^{N}(v_k-\mu(\vec{v}))^2}\right)^4}$	

3 EXPERIMENTS AND RESULTS

3.1 Experimental Setup

To assess the effectiveness of our proposed approach, we conducted experiments on four different texture datasets, organized as follows:

- **Outex** (Ojala et al., 2002a): This dataset comprises 1360 samples distributed across 68 classes, each containing 20 images, each of size 128 × 128 pixels.

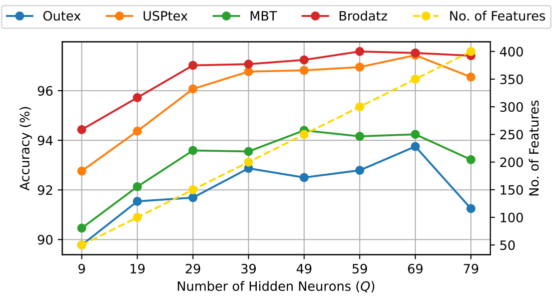

Figure 2: Classification accuracy rate (%) behavior of each evaluated dataset for various number of hidden neurons (Q) for the texture descriptor $\vec{\Omega}(Q)$.

- **USPtex** (Backes et al., 2012): The USPtex dataset includes 2292 images divided into 191 natural texture classes, with each class consisting of 12 images sized 128 × 128 pixels.
- **Brodatz** (Brodatz, 1966): This dataset contains 1776 texture samples grouped into 111 classes as structured in (Backes et al., 2013a), with each class containing 16 images of size 128 × 128 pixels.
- **MBT** (Abdelmounaime and Dong-Chen, 2013): Comprising 2464 samples, this dataset captures intra-band and inter-band spatial variations across 154 classes, each class featuring 16 images with dimensions of 160 × 160 pixels.

In this investigation, we evaluate the efficacy of the proposed technique against other methods in the literature by comparing its performance in terms of accuracy. The accuracy was obtained using Linear Discriminant Analysis (LDA) followed by a leave-one-out cross-validation strategy. In addition, the images were converted to grayscale before extracting the texture descriptors.

3.2 Parameter Analysis

Given that our proposed approach relies on a single parameter, the number of hidden neurons (Q, representing the dimension of the random projection), we evaluated its impact on the quality of the texture descriptor by measuring accuracy across four datasets for each value in $Q = 9, 19, \ldots, 79$. As shown in Fig. 2, accuracy exhibits an upward trend across all datasets up to $Q = 69$. However, at $Q = 79$, this trend stops, with a decrease in accuracy observed across all datasets, indicating that higher-dimensional projections may not yield additional improvements.

In this sense, to leverage the robustness of lower-dimensional projections, we designed the texture descriptor $\vec{\Phi}(Q_1, Q_2, \ldots, Q_L)$ that combines the learned

Table 2: Classification accuracy rates (%) of each evaluated dataset and the average accuracy of the proposed texture descriptor $\vec{\Phi}(Q_1, Q_2)$. Bold rows denote the configurations that achieved the two highest average accuracies.

(Q_1, Q_2)	**No. of Features**	**Outex**	**USPtex**	**MBT**	**Brodatz**	**Avg.**
(09, 19)	150	91.54	95.90	93.38	96.45	94.32
(09, 29)	200	92.57	96.64	94.28	97.30	95.20
(09, 39)	250	93.09	97.21	95.05	97.18	95.63
(09, 49)	300	92.79	97.08	94.81	97.47	95.54
(09, 59)	350	93.16	97.08	94.28	97.35	95.47
(09, 69)	400	93.60	97.73	94.81	97.75	95.97
(09, 79)	450	91.69	96.86	93.79	97.52	94.97
(19, 29)	250	92.65	96.99	94.40	97.24	95.32
(19, 39)	300	93.46	97.03	94.76	96.96	95.55
(19, 49)	350	92.72	97.16	95.05	97.30	95.56
(19, 59)	400	93.16	97.51	94.64	97.86	95.79
(19, 69)	**450**	**93.75**	**97.86**	**95.09**	**97.24**	**95.99**
(19, 79)	500	92.65	97.47	94.07	97.35	95.39
(29, 39)	350	93.31	97.34	95.01	97.58	95.81
(29, 49)	400	92.65	97.47	94.72	97.86	95.68
(29, 59)	450	92.79	97.60	94.44	97.97	95.70
(29, 69)	500	93.75	97.82	94.68	97.58	95.96
(29, 79)	550	92.35	97.51	94.20	97.97	95.51
(39, 49)	**450**	**94.49**	**97.77**	**94.60**	**97.75**	**96.15**
(39, 59)	500	93.53	97.56	94.93	97.97	96.00
(39, 69)	550	93.60	97.77	94.72	97.92	96.00
(39, 79)	600	92.65	97.60	94.44	97.64	95.58
(49, 59)	550	93.31	97.56	94.85	97.47	95.80
(49, 69)	600	93.53	97.99	94.93	97.69	96.04
(49, 79)	650	92.72	97.47	95.13	97.64	95.74
(59, 69)	650	92.94	97.86	94.64	98.09	95.88
(59, 79)	700	92.50	97.82	94.60	97.52	95.61
(69, 79)	750	93.01	97.64	94.20	97.97	95.71

feature vectors for each distinct number of hidden neurons. Therefore, our second experiment evaluated the performance of the proposed descriptor by measuring the average accuracy across the four datasets for every possible combination of two hidden neuron values in $\{(Q_1, Q_2) \in \mathcal{Q} \times \mathcal{Q} \mid Q_1 < Q_2\}$, thus allowing us to observe its behavior.

From Table 2, it is noteworthy that even for the same number of features, the proposed texture representation $\vec{\Phi}(Q_1, Q_2)$, produced by combining two hidden neurons, achieved higher accuracies than a single neuron representation, $\vec{\Omega}(Q)$. For instance, the combined representation $\vec{\Phi}(09, 39)$ achieved an average accuracy of 95.63%, whereas $\vec{\Omega}(49)$ achieved only 95.24%, both using 250 attributes. This indicates that the texture descriptor based on multiple lower-dimensional projections is more robust than one learned from a single higher-dimensional projection, thereby opening margins for further improvements.

Thus, these improvements are demonstrated by other combinations, such as $\vec{\Phi}(39,49)$, which achieved the highest average accuracy of 96.15% with only 450 attributes, presenting it as a robust and discriminative compact texture descriptor. This result is particularly beneficial, as reasonably small feature vectors reduce both computation and inference costs. Therefore, based on this, we selected the compact texture representations $\vec{\Phi}(39,49)$ and $\vec{\Phi}(19,69)$ both with 450 attributes, which achieved the first and the fifth average accuracies, respectively, to be compared against other methods in the literature.

3.3 Comparison and Discussions

To assess the competitiveness of our proposed texture representation, we compared it with other methods from the literature. The experimental setup was the same as the preceding section, using LDA with leave-one-out cross-validation, except for the CLBP method, which used a 1-Nearest Neighbor (1-NN) classifier.

We compared our method with three categories of descriptors: hand-engineered, RNN-based, and deep convolutional neural network (DCNN) approaches, as shown in the first, second, and third labeled row blocks of Table 3, respectively. For the DCNNs, we specifically used pre-trained models on ImageNet (Deng et al., 2009), employing them as feature extractors by applying Global Average Pooling (GAP) to the last convolutional layer, as suggested in a previous study (Ribas et al., 2024b).

Firstly, we compared our proposed approach against hand-engineered methods. Thus, as shown in Table 3 our both proposed descriptors, $\vec{\Phi}(39,49)$ and $\vec{\Phi}(19,69)$, achieved higher accuracies than hand-engineered methods across all datasets. For instance, $\vec{\Phi}(39,49)$ reached an accuracy of 94.49% on Outex, while AHP only achieved 88.31%, a notable difference of 6.18%. On USPtex, $\vec{\Phi}(39,49)$ achieved 97.77%, while AHP obtained 94.85%, an improvement of 2.92%. Furthermore, our approach obtained 97.75% on Brodatz, outperforming CLBP, which achieved 95.32%, by a difference of 2.43%. Finally, on MBT, $\vec{\Phi}(19,69)$ obtained 95.09%, while GLDM reached 92.78%, representing an increase of 2.31%. Therefore, these findings highlight the potential of our approach which uses a graph-based modeling and a simple neural network in relation to the hand-engineered approaches.

Following this, in the second part of Table 3, we present a comparison between our approach and other RNN-based methods. Notably, our proposed descriptors, $\vec{\Phi}(39,49)$ and $\vec{\Phi}(19,69)$, outperformed all RNN-based approaches on the Outex, Brodatz and MBT datasets, and ranked second on the USPtex dataset achieving an accuracy of 97.86% by $\vec{\Phi}(19,69)$, whereas the first, REE (Fares et al., 2024), achieved 98.08%, showing a small margin of 0.22% of increment. This improvement suggests that predicting the micro-graphs topological information using the pixel intensities instead of only using the pixel intensities directly as other RNN-based approaches do, allowed the network to learn more meaningful information, culminating in improved accuracies.

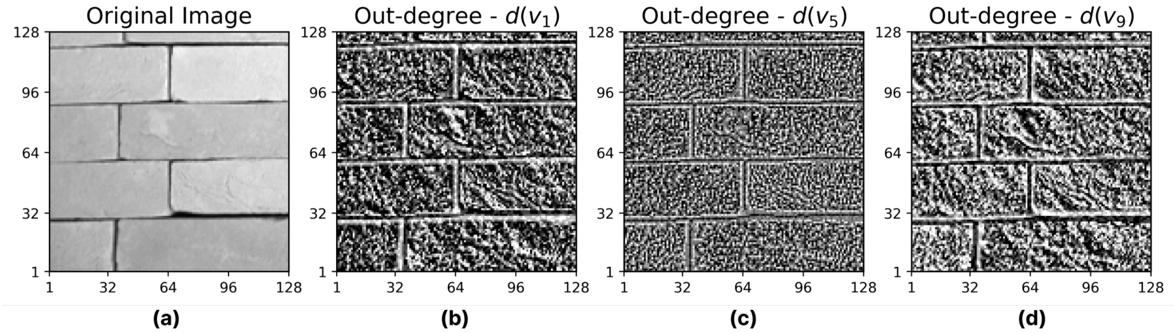

Figure 3: Illustration of enhancement of the underlying image properties by the micro-graph modeling. (a) presents the original images, whereas (b), (c) and (d) presents the visual representations of the out-degree values used as pixel intensity. The images (b) and (d) enhances the roughness information, which can hardly be seen in (a), and (c) enhances the granularity information of (a), therefore, capturing key image patterns.

Table 3: Comparison of classification accuracies of various texture analysis. A subset of these results was sourced from (Ribas et al., 2020), and (Ribas et al., 2024a). Empty cell indicate that the result is unavailable. Bold text indicates the best result, and underlined text the second-best.

Methods	# Features	Outex	USPTex	Brodatz	MBT
Hand-engineered Approaches					
GLCM (Haralick, 1979)	24	80.73	83.64	90.43	85.88
GLDM (Weszka et al., 1976)	60	86.76	92.06	94.43	92.78
Gabor Filters (Manjunath and Ma, 1996)	48	81.91	89.22	89.86	89.94
Fourier (Weszka et al., 1976)	63	81.91	67.50	75.90	–
Fractal (Backes et al., 2009)	69	80.51	78.27	87.16	–
Fractal Fourier (Florindo and Bruno, 2012)	68	68.38	59.47	71.96	–
LBP (Ojala et al., 2002b)	256	81.10	85.43	93.64	84.74
LBPV (Guo et al., 2010b)	555	75.66	54.97	86.26	73.54
CLBP (Guo et al., 2010a)	648	85.80	91.14	95.32	80.28
AHP (Zhu et al., 2015)	120	88.31	94.85	94.88	85.35
BSIF (Kannala and Rahtu, 2012)	256	77.43	77.66	91.44	79.71
LCP (Guo et al., 2011)	81	86.25	91.14	93.47	84.13
LFD (Maani et al., 2013)	276	82.57	83.55	90.99	80.20
LPQ (Ojansivu and Heikkilä, 2008)	256	79.41	85.12	92.51	74.64
CNTD (Backes et al., 2013b)	108	86.76	91.71	95.27	83.70
LETRIST (Song et al., 2018)	413	82.80	92.40	–	79.10
RNN-based Approaches					
ELM Signature (Sá Junior and Backes, 2016)	180	89.71	95.11	95.27	–
CNRNN (Ribas et al., 2020)	240	91.32	96.95	96.06	91.23
SSR^1 (Ribas et al., 2024a) (grayscale)	630	90.80	95.80	–	90.10
SSR^2 (Ribas et al., 2024a) (grayscale)	990	91.60	96.30	–	91.00
LCFNN (Ribas et al., 2024b)	330	92.13	97.21	98.09	–
REE^1 (Fares et al., 2024)	450	93.82	**98.08**	97.07	93.95
DCNN-based Approaches					
VGG19 (Simonyan and Zisserman, 2014)	512	76.62	93.19	96.79	87.42
InceptionV3 (Szegedy et al., 2016)	2048	86.40	96.77	98.54	82.14
ResNet50 (He et al., 2016)	2048	65.66	62.30	81.98	85.51
InceptionResNetV2 (Szegedy et al., 2017)	1536	85.88	96.34	**98.99**	88.60
Proposed Approach					
$\vec{\Phi}(39,49)$	450	**94.49**	97.77	97.75	94.60
$\vec{\Phi}(19,69)$	450	93.75	97.86	97.24	**95.09**

Further, in the third categorization of Table 3, we compared our technique with some DCNNs, being them: VGG19, InceptionV3, ResNet50 and InceptionResNetV2. Notably, on the Outex dataset, our descriptor $\vec{\Phi}(39,49)$ demonstrated an improvement, achieving an accuracy of 94.49%, compared to 86.40% of InceptionV3, representing a significant difference of 8.09%. This is an outstanding result, highlighting that while our texture descriptor effectively captures these textures, DCNNs exhibit certain limitations. On the USPtex dataset, our approach $\vec{\Phi}(19,69)$ achieved 97.86%, compared to 96.77% by InceptionV3, an improvement of 1.09%.

On the Brodatz dataset, the DCNNs architectures InceptionV3 and InceptionResNetV2 achieved an accuracy of 98.54% and 98.99%, respectively, being the first and second-best accuracy, while our proposed descriptors, $\vec{\Phi}(39,49)$ and $\vec{\Phi}(19,69)$, achieved 97.75% and 97.24%, ranking in third and fourth, respectively. Nevertheless, the InceptionV3 and InceptionResNetV2 used 2048 and 1536 attributes, which might be undesirable due to inference costs. Lastly, on the MBT dataset, both our approaches, $\vec{\Phi}(39,49)$ and $\vec{\Phi}(19,69)$, also presented a considerable improvement of 6.00% and 6.49%, by achieving 94.60% and 95.09%, respectively, in relation to InceptionResNetV2 accuracy of 88.60%. Here, the inefficiency of the DCNNs may be attributed to the intra-band spatial variations of the MBT textures. Thus, these results indicate the robustness of our simple and fast-learning model, compared to the presented DCNNs which are larger and have higher computational costs.

Finally, in comparison to other graph-based approaches, such as CNTD, CNRNN, SSR, and LCFNN, our proposed texture representation surpassed all of them across all evaluated datasets. For instance, while LCFNN (Ribas et al., 2024b) achieved 92.13% on Outex, our approach $\vec{\Phi}(39,49)$ reached 94.49%, a significant improvement of 2.36%, and while CNRNN (Ribas et al., 2020) achieves 91.23% on MBT, our descriptor $\vec{\Phi}(19,69)$ achieved 95.09%, an improvement of 3.86%. Therefore, these results indicate that leveraging topological measures of micro-graphs to model texture offers a more robust and discriminative approach than constructing a single graph for the entire image.

3.4 Qualitative Assessment

To complement the quantitative results presented in the preceding section, we evaluate the qualitative aspects of the proposed approach in this section, demonstrating its robustness. As micro-graph modeling is a core element of our approach, designed to enhance and extract meaningful patterns from the image, we evaluate its effectiveness in describing the image properties.

To show this, Figure 3(a) plots the original image, and Figure 3(b), 3(c) and 3(d) plot the graphical representations of the out-degree measure, $d(v)$, represented as a pixel intensity for the first (v_1), the fifth (v_5) and the ninth (v_9) vertices of the micro-graph.

In Figure 3(a), the roughness and a smooth granularity presented in the image can hardly be seen. Thus, by modeling the image using micro-graphs, and by analyzing the Figures 3(b), 3(c) and 3(d) that show the out-degree of vertices resulting from our micro-graph modeling. It can be seen that the micro-graph topological information effectively captured and enhanced the roughness and granularity, highlighting these key underlying properties of the image.

Specifically, Figure 3(b) and 3(d) presented the vertices which enhanced the roughness information, and 3(c) presented the vertex which enhanced the granularity content. Thus, these topological information enhancing different parts of the image are, therefore, predicted from the latent space, forcing the network to learn these patterns, thereby capturing the essential information.

In summary, as demonstrated in the quantitative results, our approach achieved high accuracy. This success can largely be attributed to the topological information provided into the randomized neural network. As shown in this section, the topological measures capture the essential image details, allowing the model to learn relevant and insightful texture information. This highlights the effectiveness of the micro-graph modeling in our approach.

3.5 Brazilian Plant Species Recognition

The identification of plant species is essential for many fields of knowledge, such as medicine and botany, and is commonly performed using images from leaves, seeds, and fruits, among others. However, accurately identifying species based on leaf surfaces is a challenging task due to high inter-class similarity, high intra-class variability, and environmental conditions (e.g., sun and rain) that can alter leaf characteristics. Consequently, many studies are exploring automated identification techniques based on leaf surfaces using machine learning tools to improve their performance.

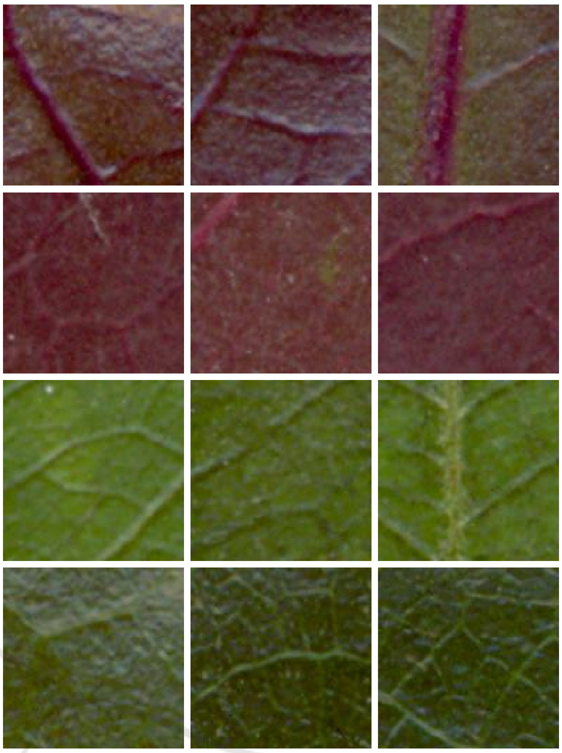

Figure 4: Plant foliar surfaces of the 1200Tex dataset. Each row presents a different class, and each column shows a distinct sample of the same class.

In this context, we evaluated our proposed methodology for plant species recognition using leaf surfaces, showing its effectiveness in an important practical application. We used the 1200Tex dataset (Backes et al., 2009), which includes 400 images of leaves divided into 20 classes, each with 20 samples. For textural analysis, these images were divided into three non-overlapping windows of 128 × 128 pixels, resulting in 1200 images. Figure 4 provides sample images from different classes for illustration. For comparison, we employed the same experimental setup as the previous section.

Table 4: Classification accuracy rates of distinct literature methods for texture analysis applied to plant species identification using foliar surfaces. Results were sourced from (Ribas et al., 2024a) or taken from their original paper.

Method	# Features	Accuracy (%)
GLDM (Weszka et al., 1976)	60	79.92
AHP (Ojansivu and Heikkilä, 2008)	120	79.17
LCP (Guo et al., 2011)	81	76.58
LFD (Maani et al., 2013)	276	74.67
LPQ (Ojansivu and Heikkilä, 2008)	256	73.00
Fourier (Weszka et al., 1976)	63	65.75
Fractal (Backes et al., 2009)	69	70.75
Gabor (Manjunath and Ma, 1996)	48	77.25
CNTD (Backes et al., 2013b)	108	83.33
RNN-CT (Zielinski et al., 2022)	240	87.08
REE^2 (Fares et al., 2024)	540	88.58
VGG19 (Simonyan and Zisserman, 2014)	512	78.33
ResNet50 (He et al., 2016)	2048	69.33
InceptionV3 (Szegedy et al., 2016)	2048	69.42
InceptionResNetv2 (Szegedy et al., 2017)	1536	67.25
Proposed Method		
$\vec{\Phi}(19, 69)$	450	**90.83**

In Table 4, we presented the results of our pro-

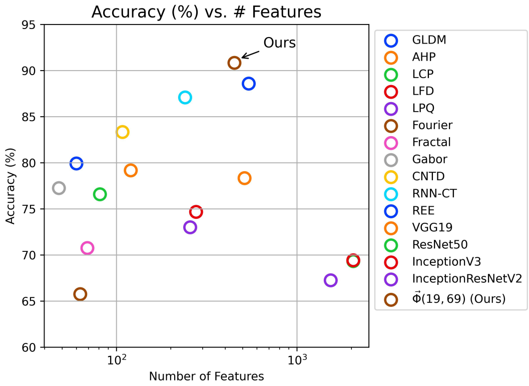

(a) 1200Tex - Impact of Number of Features

Figure 5: Results for the plant species recognition dataset. (a) Achieved accuracies (%) for the proposed texture descriptor $\vec{\Phi}(19,69)$ and other literature methods, comparing the behavior of the obtained accuracy (%) in relation to the number.

posed texture descriptor with the $\vec{\Phi}(19,69)$ configuration against other literature methods. Notably, our approach outperformed all compared methods by a considerable margin. Specifically, our texture representation achieved an accuracy of 90.83%, while the second-best method, REE (Fares et al., 2024), achieved 88.58%, representing an improvement of 2.25% and resulting in 27 additional correctly classified images. Furthermore, our approach achieved the highest accuracy while maintaining a reduced feature vector of only 450 attributes, compared to the 540 attributes for the second-best accuracy, representing a reduction of 16.67% in the feature vector size.

Additionally, we compared our approach against deep convolutional neural networks. Notably, our approach demonstrated accuracy improvements of up to 12.50% compared to the best DCNN accuracy of 78.33% achieved by VGG19 (Simonyan and Zisserman, 2014). The inefficiency of these DCNNs in this dataset may be attributed to two factors. First, the foliar surfaces in this dataset present some level of illumination variation, posing a challenge for the DCNN architectures. Second, the large feature vectors produced, even larger than the dataset size, may cause the curse of dimensionality hindering its performance.

Furthermore, Figure 5(b) shows how the number of features impacts the accuracy. Notably, methods with very low (< 100) or very high (> 600) number of features attain inadequate performance, whereas the methods ranging from 100 to 600 attributes attain promising results, such as ours. This further reinforces the sensitivity that this dataset has to the feature vector size, thus showing that a moderate number of attributes is more appropriate for achieving higher classification accuracies when building a texture representation approach.

4 CONCLUSIONS

This paper proposes a new texture representation approach that uses parameter-free micro-graph modeling, allowing for more effective capture of fine-grained details in image textures. From these micrographs, we extract topological measures to reveal diverse and invariant textural patterns within the image. These measures are then encoded using a randomized neural network in the network's learned weights, and we use the statistical summarization of the these weights as texture representation. The results demonstrate that the proposed approach is highly discriminative, surpassing several classical and deep learning-based approaches. Moreover, it outperformed other graph-based methods as well, highlighting the effectiveness of the micro-graph modeling.

To demonstrate the applicability of our approach, we also tested it on the challenging task of Brazilian plant species identification using leaf surfaces, in which it outperformed other methods by a significant margin. Therefore, these findings further highlight the potential of combining micro-graph modeling with randomized neural network for robust texture representation, providing valuable insights to the fields of computer vision and pattern recognition. As future work, our method can be adapted for color-texture and multi-scale analysis, further expanding its applicability.

ACKNOWLEDGEMENTS

R. T. Fares acknowledges support from FAPESP (grant #2024/01744-8), L. C. Ribas acknowledges support from FAPESP (grants #2023/04583-2 and

2018/22214-6). This study was financed in part by the Coordenação de Aperfeiçoamento de Pessoal de Nível Superior - Brasil (CAPES).

REFERENCES

Abdelmounaime, S. and Dong-Chen, H. (2013). New brodatz-based image databases for grayscale color and multiband texture analysis. *International Scholarly Research Notices*, 2013.

Backes, A. R., Casanova, D., and Bruno, O. M. (2009). Plant leaf identification based on volumetric fractal dimension. *International Journal of Pattern Recognition and Artificial Intelligence*, 23(06):1145–1160.

Backes, A. R., Casanova, D., and Bruno, O. M. (2012). Color texture analysis based on fractal descriptors. *Pattern Recognition*, 45(5):1984–1992.

Backes, A. R., Casanova, D., and Bruno, O. M. (2013a). Texture analysis and classification: A complex network-based approach. *Information Sciences*, 219:168–180.

Backes, A. R., Casanova, D., and Bruno, O. M. (2013b). Texture analysis and classification: A complex network-based approach. *Information Sciences*, 219:168–180.

Borzooei, S., Scabini, L., Miranda, G., Daneshgar, S., Deblieck, L., Bruno, O., De Langhe, P., De Baets, B., Nopens, I., and Torfs, E. (2024). Evaluation of activated sludge settling characteristics from microscopy images with deep convolutional neural networks and transfer learning. *Journal of Water Process Engineering*, 64:105692.

Brodatz, P. (1966). Textures: A photographic album for artisters and designerss. *Dover Publications*.

Calvetti, D., Morigi, S., Reichel, L., and Sgallari, F. (2000). Tikhonov regularization and the L-curve for large discrete ill-posed problems. *Journal of Computational and Applied Mathematics*, 123(1):423 – 446.

Cover, T. M. (1965). Geometrical and statistical properties of systems of linear inequalities with applications in pattern recognition. *IEEE Transactions on Electronic Computers*, EC-14(3):326–334.

Deng, J., Dong, W., Socher, R., Li, L.-J., Li, K., and Fei-Fei, L. (2009). Imagenet: A large-scale hierarchical image database. In *2009 IEEE conference on computer vision and pattern recognition*, pages 248–255. Ieee.

Fares, R. T. and Ribas, L. C. (2024). A new approach to learn spatio-spectral texture representation with randomized networks: Application to brazilian plant species identification. In *International Conference on Engineering Applications of Neural Networks*, pages 435–449. Springer.

Fares, R. T., Vicentim, A. C. M., Scabini, L., Zielinski, K. M., Jennane, R., Bruno, O. M., and Ribas, L. C. (2024). Randomized encoding ensemble: A new approach for texture representation. In *2024 31st International Conference on Systems, Signals and Image Processing (IWSSIP)*, pages 1–8. IEEE.

Florindo, J. B. and Bruno, O. M. (2012). Fractal descriptors based on Fourier spectrum applied to texture analysis. *Physica A: statistical Mechanics and its Applications*, 391(20):4909–4922.

Guo, Y., Zhao, G., and Pietikäinen, M. (2011). Texture classification using a linear configuration model based descriptor. In *BMVC*, pages 1–10. Citeseer.

Guo, Z., Zhang, L., and Zhang, D. (2010a). A completed modeling of local binary pattern operator for texture classification. *IEEE Transactions on Image Processing*, 19(6):1657–1663.

Guo, Z., Zhang, L., and Zhang, D. (2010b). Rotation invariant texture classification using lbp variance (lbpv) with global matching. *Pattern recognition*, 43(3):706–719.

Haralick, R. M. (1979). Statistical and structural approaches to texture. *Proceedings of the IEEE*, 67(5):786–804.

He, K., Zhang, X., Ren, S., and Sun, J. (2016). Deep residual learning for image recognition. In *Proceedings of the IEEE conference on computer vision and pattern recognition*, pages 770–778.

Huang, G.-B., Zhu, Q.-Y., and Siew, C.-K. (2006). Extreme learning machine: Theory and applications. *Neurocomputing*, 70(1):489–501.

Jagadeesh, A. V. and Gardner, J. L. (2022). Texture-like representation of objects in human visual cortex. *Proceedings of the National Academy of Sciences*, 119(17):e2115302119.

Kannala, J. and Rahtu, E. (2012). Bsif: Binarized statistical image features. In *Pattern Recognition (ICPR), 2012 21st International Conference on*, pages 1363–1366. IEEE.

Kruper, J., Richie-Halford, A., Benson, N. C., Caffarra, S., Owen, J., Wu, Y., Egan, C., Lee, A. Y., Lee, C. S., Yeatman, J. D., et al. (2024). Convolutional neural network-based classification of glaucoma using optic radiation tissue properties. *Communications Medicine*, 4(1):72.

Maani, R., Kalra, S., and Yang, Y.-H. (2013). Noise robust rotation invariant features for texture classification. *Pattern Recognition*, 46(8):2103–2116.

Manjunath, B. S. and Ma, W.-Y. (1996). Texture features for browsing and retrieval of image data. *IEEE Transactions on pattern analysis and machine intelligence*, 18(8):837–842.

Moore, E. H. (1920). On the reciprocal of the general algebraic matrix. *Bulletin of American Mathematical Society*, pages 394–395.

Ojala, T., Mäenpää, T., Pietikäinen, M., Viertola, J., Kyllönen, J., and Huovinen, S. (2002a). Outex - new framework for empirical evaluation of texture analysis algorithms. *Object recognition supported by user interaction for service robots*, 1:701–706 vol.1.

Ojala, T., Pietikäinen, M., and Mäenpää, T. (2002b). Multiresolution gray-scale and rotation invariant texture classification with local binary patterns. *Pattern Analysis and Machine Intelligence, IEEE Transactions on*, 24(7):971–987.

Ojansivu, V. and Heikkilä, J. (2008). Blur insensitive texture classification using local phase quantization. In

International conference on image and signal processing, pages 236–243. Springer.

Pao, Y.-H., Park, G.-H., and Sobajic, D. J. (1994). Learning and generalization characteristics of the random vector functional-link net. *Neurocomputing*, 6(2):163–180.

Pao, Y.-H. and Takefuji, Y. (1992). Functional-link net computing: theory, system architecture, and functionalities. *Computer*, 25(5):76–79.

Penrose, R. (1955). A generalized inverse for matrices. *Mathematical Proceedings of the Cambridge Philosophical Society*, 51(3):406–413.

Ribas, L. C., Sá Junior, J. J. M., Scabini, L. F., and Bruno, O. M. (2020). Fusion of complex networks and randomized neural networks for texture analysis. *Pattern Recognition*, 103:107189.

Ribas, L. C., Scabini, L. F., Condori, R. H., and Bruno, O. M. (2024a). Color-texture classification based on spatio-spectral complex network representations. *Physica A: Statistical Mechanics and its Applications*, page 129518.

Ribas, L. C., Scabini, L. F., de Mesquita Sá Junior, J. J., and Bruno, O. M. (2024b). Local complex features learned by randomized neural networks for texture analysis. *Pattern Analysis and Applications*, 27(1):23.

Sá Junior, J. J. M. and Backes, A. R. (2016). ELM based signature for texture classification. *Pattern Recognition*, 51:395–401.

Schmidt, W., Kraaijveld, M., and Duin, R. (1992). Feedforward neural networks with random weights. In *Proceedings., 11th IAPR International Conference on Pattern Recognition. Vol.II. Conference B: Pattern Recognition Methodology and Systems*, pages 1–4.

Simonyan, K. and Zisserman, A. (2014). Very deep convolutional networks for large-scale image recognition.

Song, T., Li, H., Meng, F., Wu, Q., and Cai, J. (2018). Letrist: Locally encoded transform feature histogram for rotation-invariant texture classification. *IEEE Transactions on Circuits and Systems for Video Technology*, 28(7):1565–1579.

Szegedy, C., Ioffe, S., Vanhoucke, V., and Alemi, A. A. (2017). Inception-v4, inception-resnet and the impact of residual connections on learning. In *Thirty-First AAAI Conference on Artificial Intelligence*.

Szegedy, C., Vanhoucke, V., Ioffe, S., Shlens, J., and Wojna, Z. (2016). Rethinking the inception architecture for computer vision. In *Proceedings of the IEEE conference on computer vision and pattern recognition*, pages 2818–2826.

Tikhonov, A. N. (1963). On the solution of ill-posed problems and the method of regularization. *Dokl. Akad. Nauk USSR*, 151(3):501–504.

Weszka, J. S., Dyer, C. R., and Rosenfeld, A. (1976). A comparative study of texture measures for terrain classification. *IEEE transactions on Systems, Man, and Cybernetics*, (4):269–285.

Xu, Z., Jiang, W., and Geng, J. (2024). Texture-aware causal feature extraction network for multimodal remote sensing data classification. *IEEE Transactions on Geoscience and Remote Sensing*.

Zhu, Z., You, X., Chen, C. P., Tao, D., Ou, W., Jiang, X., and Zou, J. (2015). An adaptive hybrid pattern for noise-robust texture analysis. *Pattern Recognition*, 48(8):2592–2608.

Zielinski, K. M. C., Ribas, L. C., Scabini, L. F. S., and Bruno, O. M. (2022). Complex texture features learned by applying randomized neural network on graphs. In *Eleventh International Conference on Image Processing Theory, Tools and Applications (IPTA), Salzburg, Austria*, pages 1–6.